Control of Three-Dimensional Island Growth with Mechanically Responsive Single-Crystal Nanomembrane Substrates

H.-J. Kim-Lee, D. E. Savage, C. S. Ritz, M. G. Lagally, and K. T. Turner*

University of Wisconsin, Madison, Wisconsin 53706, USA

(Received 16 September 2008; revised manuscript received 6 May 2009; published 5 June 2009)

Freestanding, ultracompliant crystalline-sheet substrates provide a new opportunity to control the growth of strained epitaxial films. Three-dimensional SiGe islands grown on thin silicon nanomembranes self-order as the strain field induced by initial island growth guides nucleation of subsequent islands on the opposite surface. A mechanics analysis explains this unique growth mode, possible only on ultracompliant substrates. The ordering can be tailored by manipulating the thickness and elastic properties of the membrane.

DOI: 10.1103/PhysRevLett.102.226103 PACS numbers: 81.16.Dn, 02.70.Dh, 62.25.−g

Freestanding, thin, crystalline-sheet substrates offer prospects for engineering the growth of strained epitaxial films in ways that are conceptually new in relation to the behavior on bulk substrates. Three main features contribute to these prospects. (1) Thinness: a thin (3 to 300 nm) membrane, which, by its very nature will be ultracompliant, has the ability to respond locally as well as globally to stress induced during film growth. (2) Access to two proximate surfaces: growth on one surface can influence that on the other. (3) Crystallinity: anisotropic elastic properties can be clearly expressed in the growth structures. While the unique mechanical properties of crystalline nanomembranes have previously been shown to provide new routes to fabricate 3-D nanostructures [1], the ability to exploit the distinct properties of membranes for engineering film growth has not been explored.

The growth of strained layers proceeds by the Stranski-Krastanov (S-K) mode (wetting layer followed by 3D islands) and can be influenced by substrate mechanics. The unique features of thin substrates can produce an altered subsequent 3D island size and distribution. A very graphic example is the dramatic ordering of strained S-K islands that we observe for growth of Ge on thin freestanding, single-crystal silicon nanomembranes (SiNMs) [2]; for an overview of SiNMs, see [3]. In Fig. 1, $Si_{0.36}Ge_{0.64}$ was deposited on both sides of a membrane using chemical vapor deposition to produce 3D Ge nanostressors (''hut'' islands [4]) that locally deform the substrate [5]. The unique feature here is the very good ordering of the nanostressors on a freestanding membrane, something not observed on a bulk substrate, and thus totally unexpected. The ordering is double-sided and suggests the creation of preferred nucleation sites for subsequent island formation, resulting in a chain reaction of 3D island ordering.

This Letter examines the role of substrate deformation in controlling the growth of strained epitaxial films on ultracompliant substrates. Specifically, we investigate the underlying mechanics that enables the observed ordering (Fig. 1) and explore the parameter space under which this behavior will occur. The picture of ''chain reaction of 3D island ordering'' that we develop here is appropriate for systems that have an extended nucleation regime, i.e., systems in which the nucleation density (rather than the island size) is proportional to dose. S-K systems, including the Ge-on-Si system, follow this rule [4].

The thinness of the membrane allows for the development of strain fields that extend through the thickness of the substrate during deposition and guide island nucleation. While the strain fields induced by buried islands in QD superlattices grown on bulk substrates have been extensively investigated [6,7], the ultracompliant substrates here are different. On bulk substrates, the local strain induced by the nanostressor is shared between the nanostressor and an effectively infinitely thick substrate, while on a nanomembrane, the strain is shared between the nanostressor and a thin compliant sheet. The deformation that occurs to accommodate the strain is very different in these two cases. The thinness of the nanomembrane allows the induced strain to be accommodated through different deformation modes, such as bending [8], and existing models for bulk substrates do not apply. Here, we present an

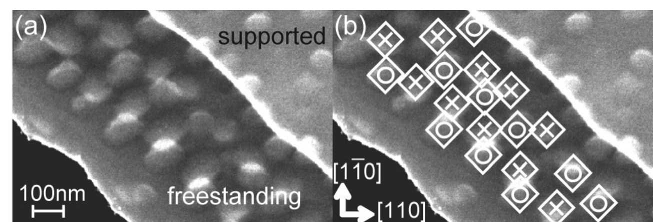

FIG. 1. (a) A Scanning electron micrograph of $Si_{0.36}Ge_{0.64}$ islands on a 23 nm thick Si membrane. The average hut size is about 70 nm, nearly three times the membrane thickness. The ordering is better on the freestanding region than the supported region. (b) The image in (a) with huts on the ''top'' and ''bottom'' of the freestanding region marked with O and X, respectively.

 © 2009 The American Physical Society

analysis of nanostressor induced strain in thin crystalline membranes, with a view towards understanding self-organization of nanostressors.

Small-strain continuum elasticity theory is suitable for predicting strain in the substrate region around a quantum dot and agrees well with atomistic calculations [9]. In the present work, elasticity calculations performed using the finite element (FE) method are used to examine the mechanics of QDs and SiNMs, as it describes well properties at near-atomic dimensions but also gives information over the long range to capture the substrate response. The present study is limited to membranes thicker than 5 nm where atomistic simulations are not necessary.

Island nucleation is controlled by the surface chemical potential, μ [7],

$$\mu = \mu_0 + \Omega\gamma\kappa_l + \Omega E_S, \tag{1}$$

where μ_0 is the chemical potential of a flat surface, Ω is the atomic volume, γ is the surface free energy per unit area, κ_l is the local curvature due to surface topography, and E_S is the local strain energy density. The formation of a hut on the surface of a SiNM causes local elastic deformation of the membrane and induces curvature and strain on the opposite surface [10]. The induced curvature is due to elastic deformation and does not contribute to the second term in Eq. (1). Thus, the distribution of elastic strain energy density alone determines the spatial variation of the surface chemical potential and the nucleation sites. In essence, the spatial modulation of strain energy generates heterogeneous nucleation sites. The observation of large ordered patches is evidence that surface diffusion is sufficiently rapid for adatoms to sample these heterogeneous sites. Note that the tensilely strained sites will preferentially attract Ge, enhancing nucleation. For alloy deposition, the Ge is expected to diffuse more rapidly than Si; thus, the same sites are decorated [11].

The spatial variation in strain energy density on the surface is quantified by the dimensionless normalized strain energy, ρ:

$$\rho(x, y) = \frac{E_S(x, y) - E_0}{E_0}, \tag{2}$$

where E_0 is the homogeneous strain energy due to the lattice mismatch strain ϵ_0 [7]. Islands are expected to nucleate preferentially at locations where ρ is minimized.

A 3-D structure consisting of a square SiNM (570×570 nm, thickness $h = 5$–120 nm) with a (001) orientation, a Ge wetting layer on each side of the membrane, and a Ge hut (height = 5 nm, hut edge length = 50 nm) on the surface of the membrane was considered to determine E_S. The strains, ϵ_{ij}, in the structure were determined using the FE method to solve the 3-D equations of small-strain linear elasticity:

$$\sigma_{ij,j} = 0, \tag{3}$$

$$\epsilon_{ij} = (u_{i,j} + u_{j,i})/2, \tag{4}$$

$$\sigma_{ij} = C_{ijkl}(\epsilon_{kl} - \epsilon_0\delta_{kl}), \tag{5}$$

where σ_{ij} are the stresses, u_i are the displacements, C_{ijkl} is the stiffness tensor, δ is the Kronecker delta, and ϵ_0 is the mismatch strain. Equations (3)–(5) are the equilibrium, strain-displacement, and constitutive equations for a case in which a mismatch strain is present and no body forces act on the structure. The appropriate values of C_{ijkl} were used in the Si and Ge regions and ϵ_0 was 4% in the Ge regions and zero in the SiNM [12]. The external surfaces of the structure are traction free, and a displacement boundary condition ($u_1 = u_2 = u_3 = 0$) was enforced at a single point located at the center of the base of the hut. The interfaces between the Si and Ge layers are bonded; thus, the displacements were continuous and the tractions balance across each interface. The strain energy density is calculated from the solution of Eqs. (3)–(5) using $E_S(x, y) = \frac{1}{2}C_{ijkl}(\epsilon_{ij} - \epsilon_0\delta_{ij})(\epsilon_{kl} - \epsilon_0\delta_{kl})$. Details of the FE calculation are provided in [12].

Figure 2(a) shows the distribution of normalized strain energy on the "bottom" surface of a 20 nm thick freestanding membrane with a single Ge hut on the "top" surface. As double-sided island growth on the freestanding membrane has never been reported, this work is the first analysis of strain on the "bottom" surface. The normalized strain energy has minimum values located just beyond the hut corners along the diagonal ($\langle 110\rangle$). The locations of these minima define preferred sites for subsequent island nucleation. The predicted locations [Fig. 2(a)] agree well with the ordering shown in Fig. 1(b).

The normalized strain energy distribution [Fig. 2(a)] and the location of the minima are determined primarily by the elastic anisotropy of the hut. When the hut is rotated by 45° [Fig. 2(b)], the locations of minima do not rotate, suggesting that the elastic anisotropy of the membrane, and not the hut shape, determines the location of the energy minima. The same orientation effects are observed for all membrane thicknesses (5–120 nm). As the elastic anisotropy dictates

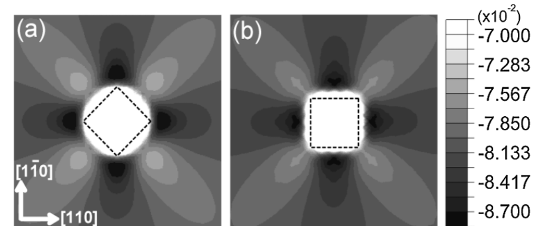

FIG. 2. Normalized strain energy distributions over a 220 nm × 220 nm area on the bottom surface of a 20 nm thick Si membrane with a 50 nm × 50 nm Ge hut on the top surface. The dashed line indicates the boundary of the hut. Two cases are shown: (a) a hut with the correct alignment relative to the crystal axes of the elastically anisotropic membrane, and (b) the hut rotated by 45° from the correct orientation.

the strain energy distribution, other island geometries, such as larger dome or smaller early-stage pointlike stress sources, will result in similar strain distribution and thus also provide an opportunity for local ordering.

To explore the role of anisotropy further, four material systems with different anisotropy ratios, $AR = 2c_{44}/(c_{11} - c_{22})$, are examined in Fig. 3. The strain energy depth, defined as the difference between the energy at the minima and the value that the energy asymptotically approaches far from the hut, increases nearly linearly with the AR of the membrane (Fig. 3). While the energy depth increases, the position of the energy minimum does not change. A greater energy depth will lead to a larger spatial variation in surface chemical potential due to strain and thus makes it more likely that the strain will determine the preferred nucleation sites over other parameters that influence nucleation position in an unstrained system, such as surface heterogeneity, deposition flux, or surface diffusion.

Elastic anisotropy has previously been shown to play a similar role in the ordering of islands in multilayer stacks on bulk substrates [7,6,13] and the trend of increasing energy depth with AR observed here is similar to bulk cases [7]. However, tetragonal vertical hut ordering has never been observed in SiGe/Si superlattices; previous work has concluded that the minima position cannot affect subsequent 3D island formation because of the small elastic anisotropy and shallow energy wells [14]. The case here is different, as the ultrathin freestanding membranes are remarkably compliant and allow off-axis alignment in the SiGe/Si system to be realized despite the weak AR. Another key difference between the nanomembrane and the multilayer systems is the effect of AR on the positions of the energy minima (i.e., distance of minima from the center of the hut). For QD superlattices, the positions of the minima move farther from the hut center as the AR of the matrix material increases [7], while in the nanomembrane system, the strain energy minima remain the same distance from the center.

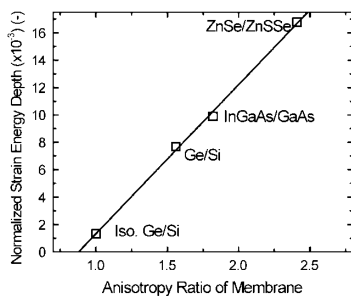

FIG. 3. Energy depth as a function of anisotropy ratio of the membrane. The anisotropy ratios of the huts are close, but not exactly the same as the corresponding membrane materials. The mismatch strain between the hut and the membrane ($h = 20$ nm) was set to 4% by changing the alloy composition. The isotropic case is based on in-plane average values of Young's modulus and Poisson's ratio.

The results above demonstrate that the elastic anisotropy of the membrane is essential to realize well ordered arrays with local anticorrelation between the huts on the top and bottom surfaces observed in Fig. 1. As island growth is stochastic and nucleation occurs simultaneously at a number of locations, rather than sequentially, the strain field is most effective at inducing local ordering. In the extended nucleation regime, islands are unlikely to nucleate close to one another over short times as a nucleated island depletes the adatom density locally.

In order to explore the ability to control the ordering on mechanically responsive substrates, we have investigated the effect of SiGe alloy composition and membrane thickness. As the Ge fraction, x, increases in the $Si_{1-x}Ge_x$ alloy, the lattice mismatch between the hut and substrate increases. Calculations for Ge fractions of 0.5, 0.64, 0.75, and 1 show that changes in alloy composition do not affect the position of the energy minima.

In contrast, the membrane thickness has a significant effect on the strain distribution. As the membrane thickness is increased, the positions of the energy minima move farther away from the hut center, and the depths of the minima decrease (Fig. 4). This behavior suggests that the distance between the islands on the top and bottom surfaces can be controlled by changing the membrane thickness, although there will be an upper limit on membrane thickness as the energy depth decreases with increasing

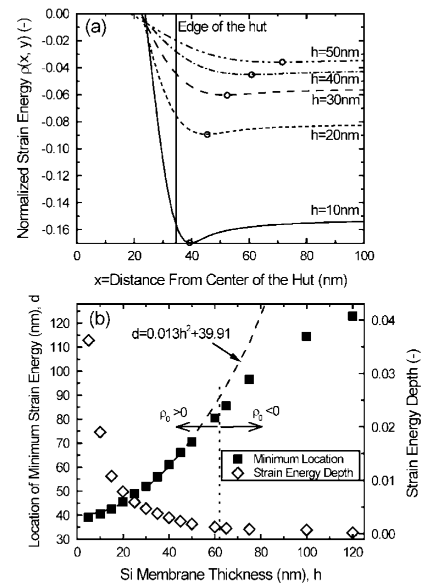

FIG. 4. (a) Strain energy along the direction of the hut diagonal for membranes with thickness from 10 to 50 nm. Circles on each curve denote the minimum. (b) The location of the minimum strain energy (square, left axis) and the strain energy depth (diamond, right axis) as a function of membrane thickness. For membranes up to about 50 nm in thickness, the position of minimum strain energy scales with the square of the membrane thickness. ρ_0, the normalized strain energy under the hut center, changes from (+) to (−) at about 60 nm.

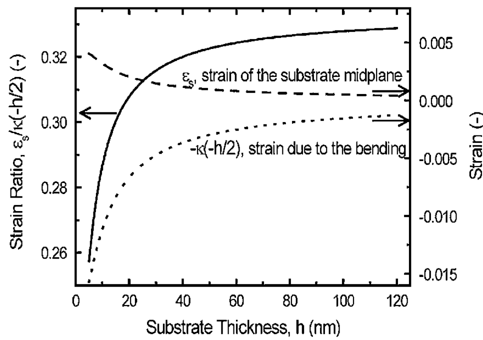

FIG. 5. The ratio (solid line, left axis) between the stretching strain in the membrane (dashed line, right axis) and the bending strain at the bottom surface of the membrane (dotted line, right axis) versus membrane thickness.

thickness. For the specific case here, the depth of energy minima decreases by more than a factor of 2 when the membrane thickness is increased from 10 to 50 nm and diminishes rapidly with increasing thickness [Fig. 4(b)]. Membrane thinness is essential to realize the self-ordering behavior described here.

The position of the strain energy minima scales with the square of membrane thickness for thicknesses up to about 50 nm [Fig. 4(b)]. The deviation from the parabolic trend above 50 nm is a result of a change in the dominant deformation mode as thickness increases. Insight into the effect of membrane thickness can be obtained from a simple layered-materials analysis. The deformed state of a layered system can be described in terms of a stretching strain, ϵ_s, and a bending curvature, κ [15]. The island can be approximated as a layer with an equivalent thickness of $h_i/3$, where h_i is the height of the island [8]. The in-plane normal strain on the bottom surface of the membrane is the sum of ϵ_s and the bending strain at the bottom surface, $\kappa(h/2)$, where h is the membrane thickness. These two strains have different signs as the Ge hut creates a tensile stretching strain while also inducing a compressive bending strain on the bottom surface. Figure 5 plots the magnitude of these two strains, calculated by a layered-materials analysis [15], for h from 5 to 120 nm with $h_i = 5$ nm. As the membrane thickness increases, the ratio of ϵ_s to $\kappa(h/2)$ increases and asymptotically approaches 0.33. The change in this ratio suggests that the effect of bending diminishes as the thickness increases and that thickness has little effect on how the mismatch strain is shared between stretching and bending strain at thicknesses greater than about 50 nm. This simple analysis illustrates the importance of membrane thickness in determining the deformation mode and confirms the change in behavior in [Fig. 4(b)] near a thickness of 50 nm.

In conclusion, we have demonstrated that thin, crystalline-sheet substrates provide a new route to engineer the self-organization of 3D nanostressors. Our analysis demonstrates the development of significant strain fields and preferred sites for subsequent 3D island nucleation around an individual 3D nanostressor due to elastic anisotropy. The locations of the nucleation sites agree well with experimental observations. The results of the analyses here illustrate two important points for realizing this type of ordering experimentally: (1) the propensity for ordering can be increased by increasing anisotropy ratio and decreasing membrane thickness, and (2) the spacing between 3D islands can be controlled by changing the membrane thickness. The manipulation of heteroepitaxy through substrate compliance provides a powerful new route for the synthesis of ordered nanostructures, and the present work provides the first analysis that explains the underlying mechanics of this process.

We thank Professor Feng Liu, Professor Michael Plesha, and Dr. Frank Flack for helpful discussions. This work is supported by NSF MRSEC (DMR-0520527) and the U.S. Department of Energy, Office of Basic Energy Sciences (DE-FG02-03ER46028).

*kturner@engr.wisc.edu

[1] M. Huang, C. Boone, C. Roberts, D. Savage, M. Lagally, N. Shaji, H. Qin, R. Blick, J. Nairn, and F. Liu, Adv. Mater. **17**, 2860 (2005).
[2] C. S. Ritz, F. S. Flack, D. E. Savage, D. Detert, P. G. Evans, M. G. Lagally, and Z. Cai, ECS Transactions **6**, 321 (2007).
[3] S. Scott and M. Lagally, J. Phys. D **40**, R75 (2007).
[4] Y. Mo, D. Savage, B. Swartzentruber, and M. Lagally, Phys. Rev. Lett. **65**, 1020 (1990).
[5] F. Liu, M. Huang, P. P. Rugheimer, D. E. Savage, and M. G. Lagally, Phys. Rev. Lett. **89**, 136101 (2002).
[6] J. Tersoff, C. Teichert, and M. G. Lagally, Phys. Rev. Lett. **76**, 1675 (1996).
[7] G. Springholz, M. Pinczolits, V. Holý, S. Zerlauth, I. Vavra, and G. Bauer, Physica E (Amsterdam) **9**, 149 (2001).
[8] M. Huang, P. Rugheimer, M. G. Lagally, and F. Liu, Phys. Rev. B **72**, 085450 (2005).
[9] C. Pryor, J. Kim, L. W. Wang, A. J. Williamson, and A. Zunger, J. Appl. Phys. **83**, 2548 (1998).
[10] B. Yang, F. Liu, and M. G. Lagally, Phys. Rev. Lett. **92**, 025502 (2004).
[11] B. J. Spencer, P. Voorhees, and J. Tersoff, Appl. Phys. Lett. **76**, 3022 (2000).
[12] See EPAPS Document No. E-PRLTAO-102-022925 for a brief summary of details of finite element calculations. For more information on EPAPS, see http://www.aip.org/pubservs/epaps.html.
[13] M. A. Makeev, W. Yu, and A. Madhukar, Phys. Rev. B **68**, 195301 (2003).
[14] V. Holý, G. Springholz, M. Pinczolitz, and G. Bauer, Phys. Rev. Lett. **83**, 356 (1999).
[15] L. B. Freund and S. Suresh, *Thin Film Materials-Stress, Defect Formation and Surface Evolution* (Cambridge University Press, Cambridge, UK, 2003).